High-Speed, High-Power Motor Design for a Four-Legged Robot Actuator Optimized using the Weighted Sum and Response Surface Methods

Tae-Woo Lee, *Student Member, IEEE*, Do-Kwan Hong, *Senior Member, IEEE*, and Tae-Uk Jung, *Member, IEEE*

***Abstract*—In this paper, a design is presented for a high-speed, high-power motor for a four-legged robot actuator that was optimized using the weighted sum method (WSM) based on the Taguchi method, and the response surface method (RSM). First, output torque, torque constant, torque ripple, and efficiency were selected as objective functions for the optimized design. The sampling method was implemented to use a mixed orthogonal array and the single response characteristics of each objective function were compared using the Taguchi method. Moreover, to consider the multi-response characteristic of the objective functions, WSM was applied. Second, the 2D finite element analysis result of the RSM was compared with that using the WSM. Finally, an experiment was carried out on the manufactured motor and the optimized model is presented here.**

***Index Terms*—Four-legged robot, Multiphysics analysis, Optimized design, Surface mounted permanent magnet synchronous motor**

I. INTRODUCTION

LEGGED robots offer the potential to navigate areas inaccessible to their wheeled counterparts. The wheeled robots may excel in terms of speed and efficiency, but they can access only flat areas. In contrast, legged robots are able to access a variety of rugged terrains such as typical for search and rescue operations in hard-to-access locations. However, this significant benefit requires complex control. Hence, legged robots are significantly costly than wheeled ones [1, 2]. These legged robots are classified according to the actuator types used.

Manuscript received November 02, 2020; accepted June 03, 2021. date of publication September 25, 2021; date of current version September 18, 2021.

This work was supported by the Industrial Strategic Technology Development Program (10070171, Development of core technology for advanced locomotion /manipulation based on high-speed/power robot platform and robot intelligence) funded By the Ministry of Trade, Industry & Energy (MI, Korea).*(Corresponding Author: Do-Kwan Hong)*

Tae-Woo Lee and Do-Kwan Hong are with the Energy and Power Conversion Engineering Department, University of Science and Technology, Changwon, 51543 Korea and Electric Machines and Drives Research Center, Korea Electrotechnology Research Institute, Changwon, 51543 South Korea (corresponding author's email: dkhong@keri.re.kr).

Tae-Uk Jung is with the Electrical Engineering Department, Kyungnam University, Changwon, 51767 South Korea (e-mail: tujung@kyungnam.ac.kr).

Digital Object Identifier 10.30941/CESTEMS.2021.00026

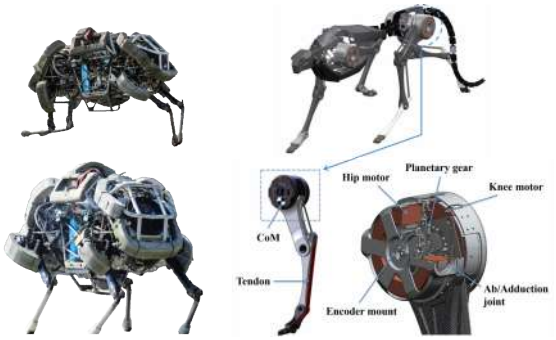

(a) (b)

Fig. 1. Hydraulic actuator and electric actuator in four-legged robots: (a) Boston Dynamics Wildcat and (b) MIT Cheetah robot.

Hydraulic actuators with engines are commonly applied for quadruped robots, which therefore require high power for heavy loads, as shown Fig. 1 (a). However, such engines come with disadvantages in terms of space and weight. These disadvantages can be resolved with the electric actuators shown in Fig. 1 (b) based on motors, but the output power of electric actuators is lower than that of hydraulic actuators [3-5]. Despite their relatively low output power, electric motors are widely used in industry and robot fields because of the great savings of space and weight.

Nowadays, permanent magnet (PM) motors can achieve high speed and high power due to development of rare earth PMs that have high residual magnetic flux density. The PM motors have other advantages such as simple magnetic circuit design, fast response, linear torque-current and speed-voltage characteristics, and have low vibration and high efficiency. In this paper, a hollow shaft-type motor based on a surface-mounted permanent-magnet synchronous motor (SPMSM) was selected to gain the advantages of PM motors. Then, two multi-objective optimization methodologies were applied. The weighted sum method (WSM) using Taguchi's orthogonal array is an easy approach when used with a low number of experimental conditions, which requires less implementation time. However, because orthogonal arrays do not test all variable combinations, the results are only relative and depend on the ratio of weighted values between objective functions [6,11,13]. Response surface methodology (RSM) allows designers to find the "best fitted" response for various

TABLE I
WINDING FACTOR, MAXIMUM PARALLEL CIRCUIT NUMBER AND FORCED VIBRATION MODE ACCORDING TO POLE AND SLOT COMBINATIONS WITH 3-PHASE, DOUBLE LAYER WINDING

Poles / Slots	2	4	6	8	10	12	14	16	18	20
3	0.866 1 | 1	0.866 1 | 1	q<1/4							
6	q>1/2	0.866 2 | 2	**	0.866 2 | 2	q<1/4					
9		q>1/2	0.866 3 | 3	0.945 * 1 | 1	0.945 * 1 | 1	0.866 3 | 3	q<1/4			
12			q>1/2	0.866 4 | 4	0.933 2 | 2	**	0.933 2 | 2	0.866 4 | 4	q<1/4	
15				q>1/2	0.866 5 | 5	**	0.951 * 1	0.951 * 1	**	0.866 5
18					q>1/2	0.866 6 | 6	0.902 2 | 2	0.945 2 | 2	**	0.945 2 | 2
21						q>1/2	0.866 7 | 7	0.890 1 | 1	**	0.953 * 1 | 1
24							q>1/2	0.866 8 | 8	**	0.933 4 | 4

Winding factor	
Max. parallel circuit number	Forced vibration mode

* Unbalance magnetic force
** Unfeasible 3-phase winding

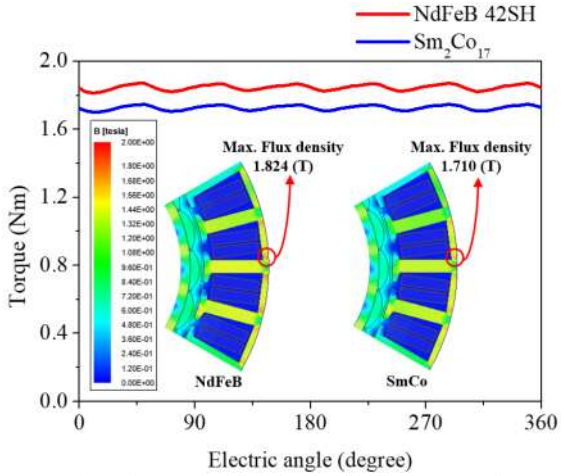

Fig. 2. Comparison of torque and flux density distribution according to magnet materials for the initial model.

objective functions with an overall prospect of the performance according to the behavior of the parameters within a design space. However, the quality of the optimized model depends on the size of the space. If the range of design variables is narrow, an optimal condition is not detected. This is guaranteed because the full design region is not explored. Hence, it is important to select the proper range of design variables by screening and search for the specific levels of important variables needed to produce an optimum response [7,8,11].

II. DESIGN AND ANALYSIS FOR OPTIMIZATION

A. Selection of Pole-Slot Combination and Magnets

When designing a motor, the pole-slot combination should be selected considering the electrical and mechanical characteristics. If the winding factor increases, better electrical performance can be achieved because of increase in the magnetic flux utilization between the rotor and the stator. Concentrated winding (which is a simple configuration with short end-winding length) is widely applied instead of distributed winding to reduce loss, unless it is an ultra-high-speed motor in SPMSM. Moreover, double-layer winding in a slot can increase utilization. The greatest common divisor (GCD) of the number of poles and slots can predict the approximate forced vibration mode because the electromagnetic pressures generated by the stator and rotor are most important. Based on the pole-slot combinations, the maximum number of parallel circuits can also be changed. The winding factor, maximum parallel circuit number, and forced vibration mode according to pole-slot combinations of three phases and double-layer winding, are represented in Table I. The higher winding factor and the forced vibration mode represent better conditions [9, 10]. In this paper, the pole-slot combination chosen was a 20 pole-24 slot model with reference to the winding factor, forced vibration mode, and maximum number of parallel circuits.

Deciding what material to use in the motor application is important, especially when it comes to permanent magnets such as samarium-cobalt (SmCo) and neodymium-iron-boron (NdFeB). The SmCo magnets can be used in applications for operation at high temperature. The SmCo magnets are not recommended in applications that require high structural stability because these magnets tend to flake off relatively

TABLE II
REQUIRED DESIGN SPECIFICATIONS OF THE ACTUATOR

Item	Value	Item	Value	Item	Value
Torque (Nm)	2	Rated speed (rpm)	3,000	Rated power (W)	620

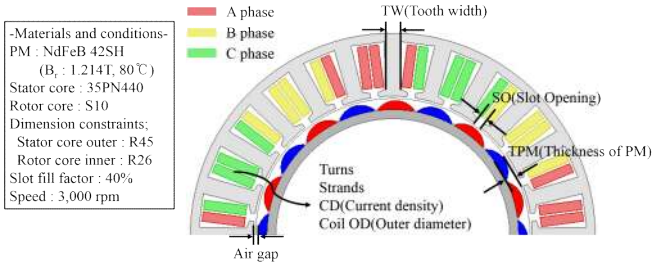

Fig. 3. Design variables of the initial model.

TABLE III
CONTROL FACTORS AND NOISE FACTOR

Control factor		Level 1	Level 2	Level 3
A	Turns	7	8	-
B	Air gap*	0.9	1	1.1
C	TPM*	1.9	2	2.1
D	TW*	2.9	3	3.1
E	SO*	1.4	1.5	1.6
F	Strands	3	4	5
G	CD**	4	6	8
H	Coil OD*	0.6	0.65	0.7

* Unit mm, ** Unit A_{rms}/mm^2

Noise factor		Level 1	Level 2
N	Analysis interval (Mech. Angle)	0.5°	0.2°

TABLE IV
L18 ($2^1 \times 3^7$) MIXED ORTHOGONAL ARRAY WITH SIGNAL/NOISE RATIO

No.	A	B	C	D	E	F	G	H	Torque SNR	Efficiency SNR	Torque constant SNR	Torque ripple SNR
1	7	0.9	1.9	2.9	1.4	3	4	0.6	-7.66	38.44	-16.76	-12.52
2	7	0.9	2.0	3.0	1.5	4	6	0.65	0.06	39.13	-16.58	-7.42
3	7	0.9	2.1	3.1	1.6	5	8	0.7	5.84	39.30	-16.62	-6.93
4	7	1.0	1.9	2.9	1.5	4	8	0.7	3.31	39.21	-17.21	-6.83
5	7	1.0	2.0	3.0	1.6	5	4	0.6	-3.37	38.99	-16.9	-5.74
6	7	1.0	2.1	3.1	1.4	3	6	0.65	-2.57	38.98	-16.71	-5.32
7	7	1.1	1.9	3.0	1.4	5	6	0.7	2.48	39.29	-17.48	-2.61
8	7	1.1	2.0	3.1	1.5	3	8	0.6	-2.12	38.98	-17.24	0.17
9	7	1.1	2.1	2.9	1.6	4	4	0.65	-4.09	38.96	-17.20	-4.00
10	8	0.9	1.9	3.1	1.6	4	6	0.6	-0.37	39.11	-15.49	-3.97
11	8	0.9	2.0	2.9	1.4	5	8	0.65	5.41	39.28	-15.66	-9.47
12	8	0.9	2.1	3.0	1.5	3	4	0.7	-3.31	38.92	-15.31	-9.05
13	8	1.0	1.9	3.0	1.6	3	8	0.65	0.71	39.13	-15.93	-4.56
14	8	1.0	2.0	3.1	1.4	4	4	0.7	-1.17	39.17	-15.67	-2.18
15	8	1.0	2.1	2.9	1.5	5	6	0.6	1.29	39.20	-15.76	-6.11
16	8	1.1	1.9	3.1	1.5	5	4	0.65	-1.20	39.23	-16.25	0.49
17	8	1.1	2.0	2.9	1.6	3	6	0.7	-0.67	39.13	-16.19	-3.32
18	8	1.1	2.1	3.0	1.4	4	8	0.6	1.62	39.16	-16.00	-1.66

TABLE V
WEIGHTED VALUES CALCULATED BY AHP

Symbol	Parameter	Value
ω_1	Torque weighted values	0.45
ω_2	Torque constant weighted values	0.27
ω_3	Torque ripple weighted values	0.10
ω_4	Efficiency weighted values	0.18

easily. Fig. 2 shows a comparison of torque and flux density distribution according to magnet materials for the initial 20 pole-24 slot model. Based on Fig. 2, the NdFeB magnets were more suitable considering operating conditions and cost.

B. Weighted Sum Method

Before optimization, the output torque, torque constant, torque ripple, and efficiency were selected as objective functions based on the required design specifications shown in Table II. The design variables were primarily selected by separating the mechanical elements such as air gap, thickness of permanent magnet, and slot-opening determined shapes and the electrical elements such as current density, coil outer diameter, number of turns and number of strands, which affect the electric performance, as shown Fig. 3. As the number of design variables increases, a full factorial design may become very onerous to complete. Therefore, the sampling method chosen must be appropriate. Therefore, the L18 ($2^1 \times 3^7$) mixed orthogonal array and Taguchi method were applied in this paper to maximize the effect of the results while minimizing the data set.

The design variables selected were chosen as control factors and the two-dimensional (2D) finite element analysis (FEA) intervals were selected as noise factors, as shown in Table III. Based on the mixed orthogonal array, 2D FEA was performed and the signal-to-noise ratio (S/N ratio, SNR) was calculated in terms of the results using (1) and (2), as shown Table IV.

Smaller-is-better

$$SNR_{SB} = -10 \log \left[\frac{1}{n} \sum_{i=1}^{n} y_i^2 \right] \quad (1)$$

Larger-is-better

$$SNR_{LB} = -10 \log \left[\frac{1}{n} \sum_{i=1}^{n} \frac{1}{y_i^2} \right] \quad (2)$$

(n : the number of responses, y_i : output)

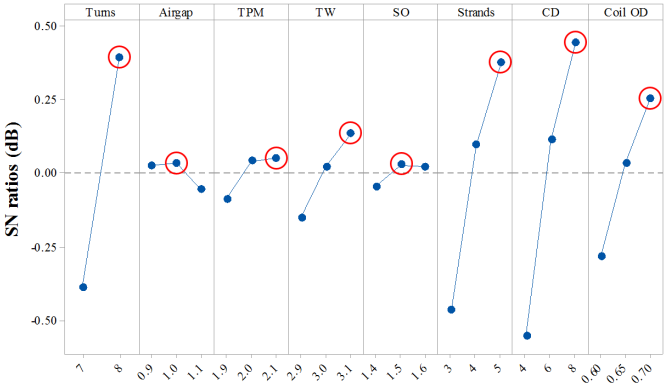

Fig. 4. Main effects plot for MRSN ratios.

TABLE VI
CENTRAL COMPOSITE DESIGN ARRAY WITH THREE VARIABLES

No.	A	B	C	Torque (Nm)	Torque const. (Nm/A_{rms})	Torque ripple (%)	Efficiency (%)
1	1.12	2.12	2.88	1.961	0.148	2.10	92.11
2	1	2	3	2.038	0.154	2.02	92.25
3	1.12	2.12	3.12	1.998	0.151	1.38	92.34
4	1	1.8	3	1.979	0.149	2.00	92.12
5	0.88	2.12	2.88	2.148	0.162	2.67	92.26
6	1.2	2	3	1.879	0.142	1.40	92.07
7	0.88	1.88	3.12	2.116	0.159	1.91	92.37
8	1.12	1.88	3.12	1.933	0.146	1.33	92.20
9	1.12	1.88	2.88	1.890	0.142	1.89	91.96
10	0.88	2.12	3.12	2.212	0.167	2.11	92.52
11	1	2	3.2	2.068	0.156	1.39	92.43
12	0.88	1.88	2.88	2.064	0.156	2.57	92.12
13	0.8	2	3	2.207	0.166	2.55	92.36
14	1	2	2.8	1.993	0.150	2.47	92.03
15	1	2.2	3	2.110	0.159	2.08	92.37

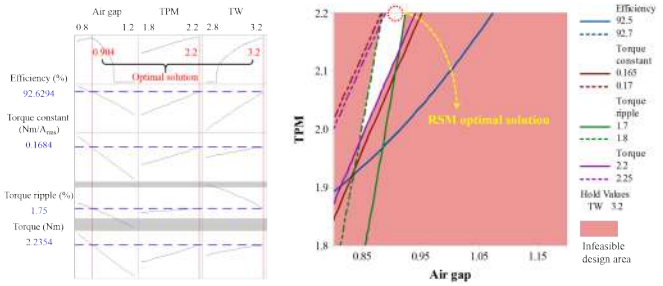

Fig. 5. Results of the optimal solution and overlaid contour plot with RSM.

The Taguchi method can derive a robust model for single response characteristics but it cannot provide an optimal model

TABLE VII
THE RESULTS OF 2D FEA FOR EACH OPTIMIZED DESIGNS AT 3,000 RPM

Item	Output torque (Nm)	Torque constant (Nm/A_{rms})	Torque ripple (%)	Efficiency (%)
Initial model	1.847	0.163	3.08	92.548
WSM model	2.095	0.158	1.63	92.432
RSM model (1mm airgap)	2.143	0.161	1.35	92.593

(Mechanical loss is not included in the efficiency.)

considering multiple response characteristics. Hence, the weight sum method (WSM) was applied. First, the result of the S/N ratios were normalized through (3) because the S/N ratios of each objective function have different scales. After adjusting the notionally common scale by normalization, the weighted values calculated by the analytic hierarchy process (AHP), as shown in Table V, were applied to the results using (4) to obtain a multi-response signal-to-noise (MRSN) ratio [11-13].

$$Z_{SN_p} = \frac{X_{SN_p} - \mu_{SN_p}}{\sigma_{SN_p}} \tag{3}$$

$$MRSN\ \ Ratio = \sum_{i=1}^{p} \omega_i Z_{SN_p} \tag{4}$$

(X_{SN_p} :SN Ratio, μ_{SN_p} : mean, σ_{SN_p} : standard deviation)

The optimized model can be projected using a combination of the maximum values for the S/N ratios of each control factor from Fig. 4. When the results from the initial model and WSM model were compared, the output torque of the latter was about 13.4% greater and the torque ripple was about 47.07% less.

C. Response Surface Method

The response surface method (RSM) is a collection of mathematical and statistical techniques strictly related to design of experiments (DOE). The main idea is to use the results of the DOE run to create an approximation of the response variable over the design space. The approximation is called a response surface or meta-model, such as a polynomial function, and can be built for any output variable [11]. Central composite design (CCD) was applied in this work because it can be used to construct the second-order model efficiently. Three sensitive variables affecting geometry (A: the air gap, B: the thickness of PM (TPM), and C: the tooth width, TW) were chosen and other design variables and objective functions were kept the same as in the WSM model. Table VI presents a CCD array with these sensitive variables and the results of 2D FEA for each case. Fig. 5 shows the best combination under the constraints and conditions. When compared with the results of WSM, the RSM results were better; moreover, the meta-models of each objective function were obtained using (5)-(8).

$$\begin{aligned} Torque = & -0.92+0.63A+0.02B+1.6C+0.14A^2 \\ & +0.17B^2-0.18C^2-0.39AB-0.31AC \end{aligned} \tag{5}$$

$$Torque=0.92$$

$$\begin{aligned} Torque\ constant = & -0.07+0.05A-0.002B+0.12C+0.01A^2 \\ & +0.013B^2-0.014C^2-0.029AB-0.024AC \end{aligned} \tag{6}$$

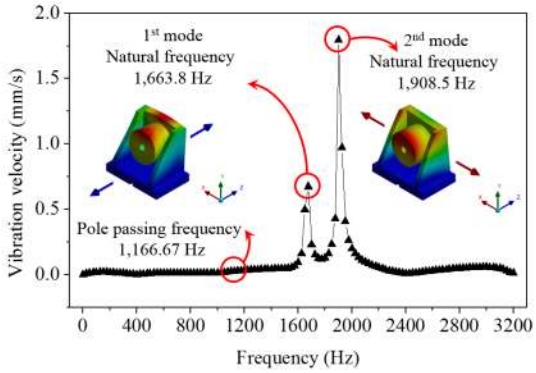

Fig. 6. Vibration velocity frequency response at 3,500 rpm.

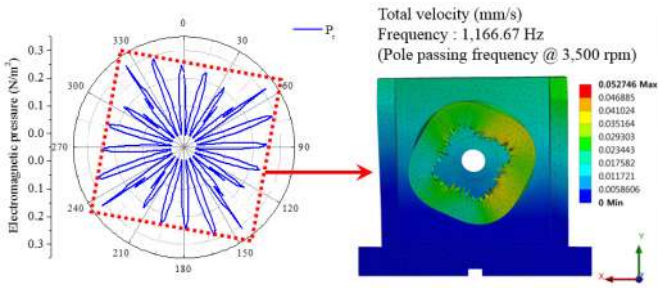

Fig. 7. Electromagnetic pressure and total velocity at 3,500 rpm.

$$\begin{aligned} Torque\ ripple = & -11.45-0.12A+0.43B+12.04C \\ & -1.32A^2-2.45C^2 \end{aligned} \tag{7}$$

$$\begin{aligned} Efficiency = & 84.69+1.79A+0.614B+2.85C \\ & -0.71A^2-0.25C^2-0.36AC \end{aligned} \tag{8}$$

The adjusted determination coefficient of each response, which shows the reliability of each of four meta-models, was found to be 0.9988, 0.9988, 0.9893, and 0.9991. For productivity, the air gap was changed from 0.904 to 1 mm, with a margin. Table VII shows the comparison with the initial model, WSM model, and RSM model with a 1 mm air gap.

D. Mechanical Analysis of the Optimized Model

In rotating machines, if the electrical exciting frequency caused by magnetic flux between stator and rotor matches the natural frequency of the motor and support structure, a large amount of vibration and noise appear in the structure. Hence, the avoidance of resonance is essential. A forced vibration analysis was carried out by mapping the harmonic components of the pole passing frequency to the end of teeth of the stator. Fig. 6 presents the result of the frequency response for vibration velocity at the side-load bearing support during the maximum speed (3500 rpm) of this motor. The pole passing frequency f_p is given by

$$f_p = 2f_e = 2\frac{n}{60}\cdot\frac{p}{2} \tag{9}$$

where n is the rotational speed (rpm) and p is the number of poles. The pole passing frequency, which is the twice the electrical frequency f_e, is the mechanical exciting frequency (1166.67 Hz, 20 poles). It was separated from the peak of 1st and 2nd natural frequencies. We verified that this motor was not affected by resonance even though it was operated at maximum

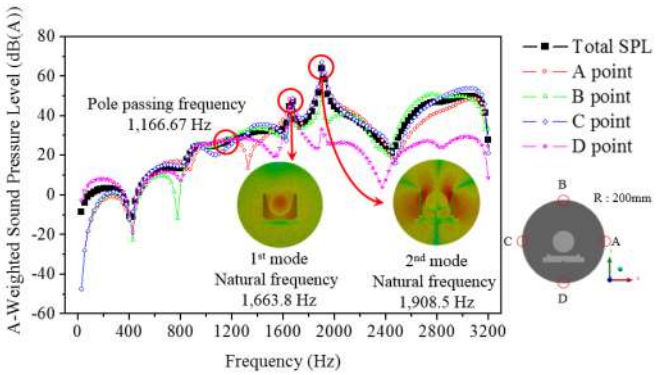

Fig. 8. Results of the acoustic analysis according to frequency at 3,500 rpm.

speed.

The forced vibration mode can be determined by the GCD of the number of poles and slots in Table I. The higher the order of the forced vibration mode, the lower the probability that it will coincide with the natural frequency of the motor, and the more likely it is to avoid resonance. For this paper, the 4-forced vibration mode was selected by the pole-slot combination. The electromagnetic pressure P_r was calculated as in (10)-(12) to use the flux density B_r, B_t of the radial and tangential directions based on the Maxwell stress method.

$$P_r = \frac{1}{2\mu_0}\left(B_r^2 - B_t^2\right) \tag{10}$$

$$B_r = B_x \cos\theta + B_y \sin\theta \tag{11}$$

$$B_t = -B_x \sin\theta + B_y \cos\theta \tag{12}$$

Fig. 7 shows the electromagnetic pressure and total velocity at the maximum speed. As expected, the forced vibration mode was rectangular due to the electromagnetic force at the ends of the stator teeth.

The vibration velocity of the harmonic response on the surface of the motor generates noise energy in the air. An acoustic analysis was performed by mapping the vibration velocities on the surface of the motor according to frequencies transmitted to the external air. The result of the acoustic analysis indicated that the A-weighted sound pressure levels, which were calibrated, were higher at the first and second natural frequencies and that the sound pressure levels were relatively small at the pole passing frequency. Fig. 8 shows the sound pressure level relative to the frequency and the results of the measurement with a virtual microphone placed on the surface of a sphere with the noise emitted in each direction.

III. Experimental Validation

In Section II, the RSM model had the best performance under the same conditions. Hence, the proposed prototype 20 pole-24 slot motor was fabricated as shown in Fig. 9. The performance test used a back-to-back dynamo system with a load motor (Siemens, 1FT7044) and a human machine interface (HMI). The data acquisition system included a power analyzer (Yokogawa, WT1800), a 5 Nm-rated torque sensor (Kistler, 4503B), and other components as shown in Fig. 10 [9]. During this experiments, 55 V DC current was supplied to the test

Fig. 9. Proposed prototype 20 pole-24 slot motor.

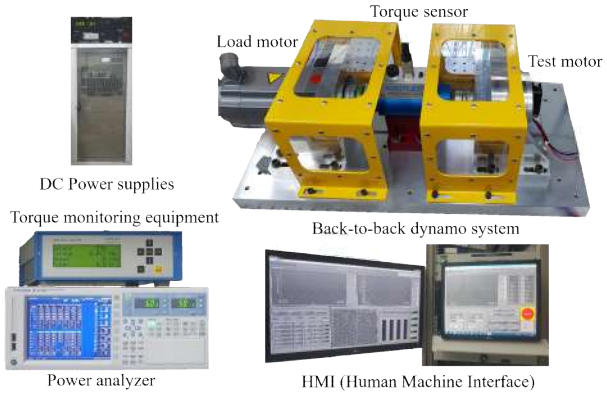

Fig. 10. Configuration of the performance test equipment.

TABLE VIII
Comparison between 2D FEA and Experimental Results

Speed (rpm)	500	1,000	1,500	2,000	2,500	3,000
Experiment (%)	71.51	81.33	84.73	87.08	88.00	87.79
2D FEA* (%)	74.53	82.18	84.94	86.30	87.06	87.52
Error (%)	4.05	1.03	0.25	0.91	1.08	0.31

* Mechanical loss is included in efficiency

motor and the current was limited to 1.8 times the motor power rating to obtain the motor operating range. The full load performance maps of the proposed motor are plotted in Fig. 11 (a)-(d). Table VIII shows a comparison between the 2D FEA and experimental results for efficiency according to speed. We assumed that the mechanical loss is 6% of the output power.

Fig. 12 presents the configuration of vibration and noise test equipment. The setup included an FFT analyzer (Bruel & Kjaer), tachometer, microphone and accelerometer. Fig. 13 and Fig. 14 show the results of the FFT and order tracking analysis for vibration acceleration during run-up (0–3500 rpm). It was found that the vibration acceleration was mainly generated at the pole pass frequency, as expected. There was a rotational frequency in the experiment but it could be eliminated through rotor balancing. Fig. 15 shows the vibration velocities according to speed and measuring points (which are drive end: DE and non drive end: NDE). It can be seen that continuous operation is possible because it belongs to the A area of Group 2 (1.4 mm/s or less) according to ISO 10816-3 (the standard for measurement and evaluation of machine vibrations). Fig. 16 presents the result of a 1/3 octave analysis of the sound pressure

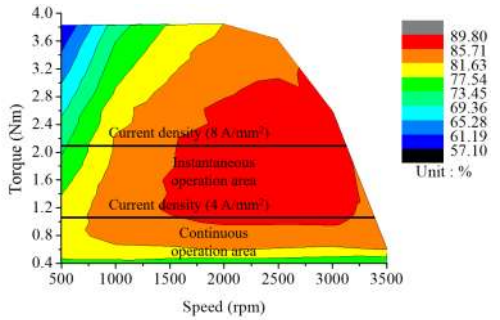

(a) Efficiency

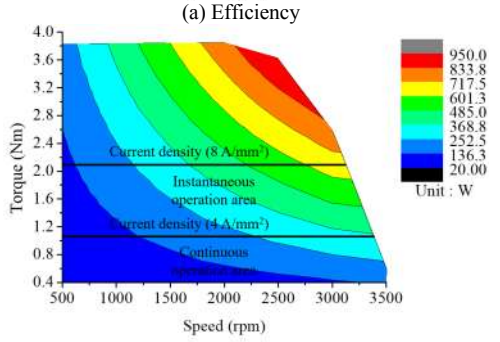

(b) Output power

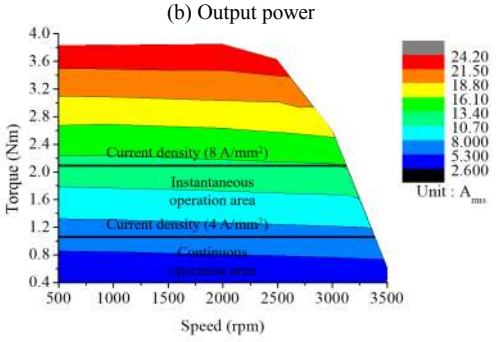

(c) Current

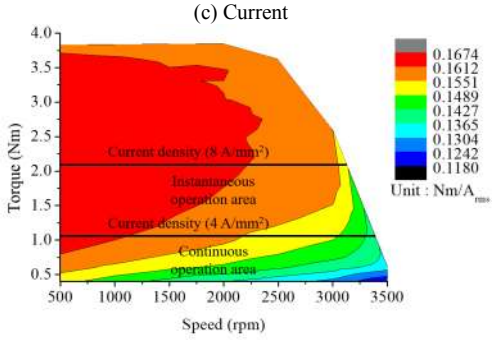

(d) Torque constant

Fig. 11. Measured performance maps of the prototype motor.

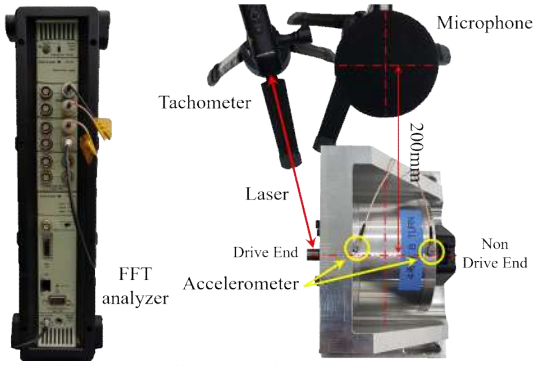

Fig. 12. Configuration of vibration and noise test equipment.

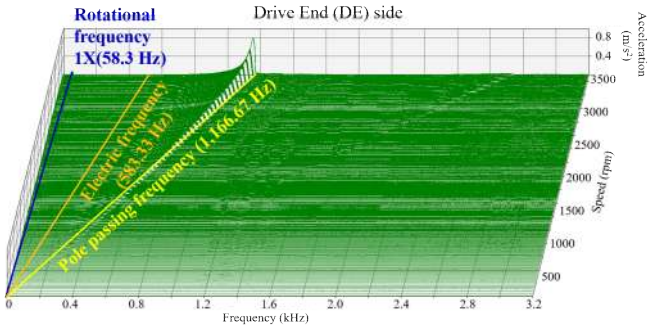

Fig. 13. Results of the FFT analysis for vibration acceleration at DE during run-up (0–3500 rpm).

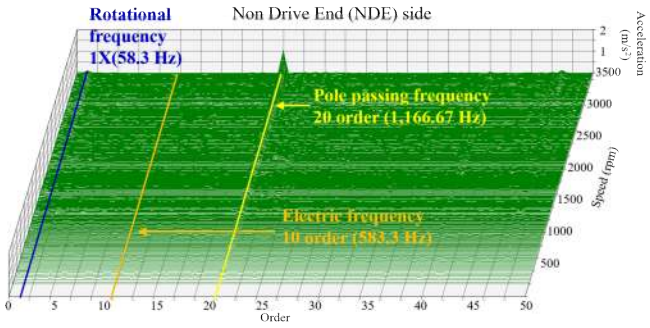

Fig. 14. Results of the order tracking analysis for vibration acceleration at NDE during run-up (0–3500 rpm).

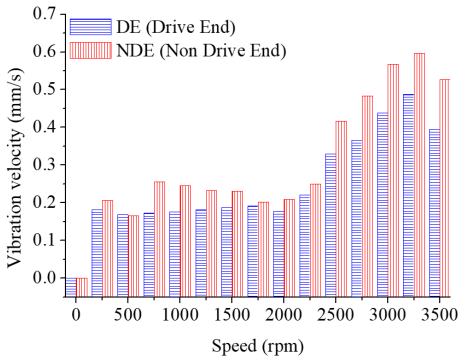

Fig. 15. Vibration velocity according to speed.

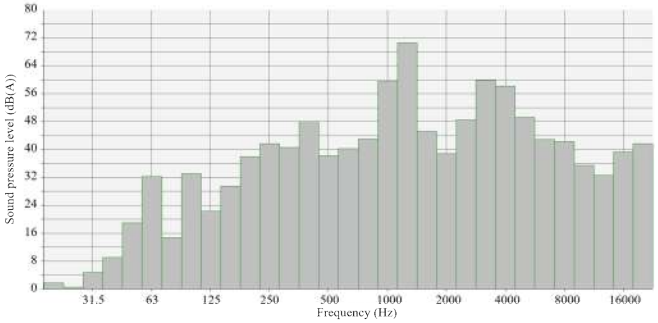

Fig. 16. Results of the 1/3 octave analysis of sound pressure level at maximum speed (3500 rpm).

level at maximum speed (3500 rpm). When the electric motor was driven at the maximum speed, the sum of the pressure levels in the audible frequency band was about 70 dB (A). Considering that the sound pressure level of normal conversation is between 60 and 70 dB (A), it can be seen that the noise of the motor was not loud.

IV. CONCLUSIONS

In this paper, the design and a prototype of a high-speed, high-power, hollow-shaft-type SPMSM is presented considering multi-response characteristics such as output torque, torque constant, torque ripple, and efficiency. To consider its multi-response characteristics, 2D electromagnetic analysis using WSM and RSM were employed to optimize the design process. When the results of the two optimization methodologies were compared, the performance of RSM optimized model was better than with the WSM model. It was confirmed that the optimized model met the design specifications. In addition, mechanical analyses such as the forced vibration and acoustic analysis of the optimized model, were conducted at the maximum operating speed. The vibration and noise were maximal at the pole passing frequency, which is the main excitation frequency. In addition, a prototype of the proposed model was fabricated and performance tests were carried out. The average error rate for efficiency was 1.27% between simulation and experiment. It was confirmed that this motor could operate continuously based on its vibration velocity and noise level. The optimized design, multiphysics analysis, and experimental tests of this motor for application to four-legged robots were all successful.

REFERENCES

[1] J. Zico Kolter and Andrew Y. Ng, "The Stanford LittleDog: A learning and rapid replanning approach to quadruped locomotion", *The International Journal of Robotics Research*, Vol. 30, No. 2, pp. 150-174, Jan. 2011.

[2] T. Hojnik, R. A. Dungavell, P. D. Flick and J. M. Roberts, "Wheeled Rovers With Posable Hubs for Terrestrial and Extraterrestrial Exploration," *IEEE Access*, vol. 8, pp. 154318-154328, Aug. 2020.

[3] L. Pang, Z. Cao, J. Yu, P. Guan, X. Rong and H. Chai, "A Visual Leader-Following Approach With a T-D-R Framework for Quadruped Robots," *IEEE Transactions on Systems, Man, and Cybernetics: Systems*, vol. 51, no. 4, pp. 2342-2354, Apr. 2021.

[4] Evan Ackerman (2013, Oct.), "Whoa: Boston Dynamics Announces New WildCat Ouadruped Robot", IEEE spectrum, NY.

[5] S. O. Seok, A. Wang, D. Otten and S. B. Kim, "Actuator Design for High Force Proprioceptive Control in Fast Legged Locomotion", *2012 IEEE/RSJ International Conference on Intelligent Robots and Systems*, pp. 1970-1975, Oct. 2012.

[6] Stephanie Fraley, Mike Oom, Ben Terrien and John Zalewski, "Design of experiments via taguchi methods: orthogonal arrays", Dec. 2006.

[7] Sung-Il Kim, Jung-Pyo Hong, Young-Kyoun Kim, Hyuk Nam and Han-Ik Cho, "Optimal design of slotless-type PMLSM considering multiple responses by response surface methodology," *IEEE Transactions on Magnetics*, vol. 42, no. 4, pp. 1219-1222, Apr. 2006.

[8] H. T. Wang *et al*., "Optimal Design of MAMR and HAMR by Applying Response Surface Methodology," *IEEE Transactions on Magnetics*, vol. 49, no. 6, pp. 2719-2722, Jun. 2013.

[9] D. K. Hong, W. Hwang, J. Y. Lee and B. C. Woo, "Design, Analysis, and Experimental Validation of a Permanent Magnet Synchronous Motor for Articulated Robot Applications," *IEEE Transactions on Magnetics*, vol. 54, no. 3, pp. 1-4, Mar. 2018.

[10] S. E. Skaar, Ø. Krøvel, R. Nilssen, "Distribution, coil-span and winding factors for PM machines with concentrated windings", *Proceedings of ICEM 2006*, pp. 2-5, 2006.

[11] M. Cavazzuti, *Optimization Methods: From Theory to Design Scientific and Technological Aspects in Mechanics*, 1st ed., Springer Science & Business Media 2013, pp. 21~74.

[12] H. K. Park, B. Y. Yang, S. B. Rhee and B. I. Kwon, "Novel Design of Flux Barrier in IPM type BLDC motor by considering the Multi-response Taguchi Method", *The transactions of The Korean Institute of Electrical Engineers*, Vol. 56, No. 3, pp. 498~505, Mar. 2007.

[13] M. R. Chen, P. Chiang and L. Lin, "Device robust-design using multiple-response optimization technique," *Proceedings of 5th International Workshop on Statistical Metrology*, pp. 46-49, Jun. 2000.

Tae-Woo Lee (S'18) was born in Changwon, South Korea. He received the B.S. degree in electrical engineering from the Changwon National University, Changwon, South Korea in 2014. He is currently pursuing a Ph.D. degree (integrative program) in energy and power conversion engineering at the University of Science and Technology, Changwon, South Korea.

From 2014 to 2017, he was an engineer with Hyundai Heavy Industry, Ulsan, South Korea. Since 2017, he has been with the Electric Machines and Drives Research Center, Korea Electrotechnology Research Institute, Changwon, South Korea, as a student researcher. His research interests include the design, optimization, analysis, and experimental validation of high speed-high power electric machines for various industrial and electric propulsion applications, such as magnetic gears and electrically driven machines.

Mr. Lee is a student member of the Institute of Electrical and Electronics Engineers (IEEE), USA and a member of the Korean Institute of Electrical Engineers (KIEE), and Korean Society for Precision Engineering (KSPE), South Korea. He was a recipient of the International Conference of Asian Union of Magnetics Societies (IcAUMS) Best Poster Award in 2018, and the Korean Institute of Electrical Engineers (KIEE) Paper Award in 2018 and 2020.

Do-Kwan Hong (M'08–SM'19) was born in Busan, South Korea. He received the B.S., M.S., and Ph.D. degrees in mechanical engineering from the Dong-A University of Busan, South Korea in 1998, 2000, and 2004, respectively.

Since 2004, he has been with the Electric Machines and Drives Research Center, Korea Electrotechnology Research Institute, Changwon, South Korea, as a Principal Researcher. Since 2015, he has been with the Energy and Power Conversion Engineering, University of Science and Technology, Changwon, South Korea, as an Associate Professor. His research interests include design, multiphysics performance analysis, and experimental validation of the performance of high-speed high-torque high-power machines for a variety of industrial applications and all-electric propulsion applications, such as for magnetic gears and electrically driven machines.

Dr. Hong is a Senior Member of the Institute of Electrical and Electronics Engineers (IEEE), USA and a member of the Korean Institute of Electrical Engineers (KIEE), Korean Society of Mechanical Engineers (KSME), Korean Society for Noise and Vibration Engineering (KSNVE), and Korean Society for Precision Engineering (KSPE), South Korea. He is a reviewer of IEEE transactions on magnetics, etc.

Tae-Uk Jung (M'99) was born in Masan, South Korea, in 1970. He received the B.S., M.S., and Ph.D. degrees in electrical engineering from Busan National University, Busan, South Korea, in 1993, 1995, and 1999, respectively.

Between 1996 and 2005, he was a Chief Research Engineer with the Laboratory of LG Electronics, South Korea. Between 2006 and 2007, he was a Senior Research Engineer at the Korea Institute of Industrial Technology, South Korea. Since 2007, he has been a professor at Kyungnam University. His research interests include high-efficiency motor design and applications.

Prof. Jung is a member of the Institute of Electrical Engineers of Korea (KIEE) and the Institute of Electrical and Electronics Engineers (IEEE), USA.